How to cite: *Angew. Chem. Int. Ed.* **2022**, *61*, e202203783
International Edition: doi.org/10.1002/anie.202203783
German Edition: doi.org/10.1002/ange.202203783

Supramolecular Polymerization

Expanding the Scope of Metastable Species in Hydrogen Bonding-Directed Supramolecular Polymerization

*Jonas Matern, Zulema Fernández, Nils Bäumer, and Gustavo Fernández**

Abstract: We reveal unique hydrogen (H-) bonding patterns and exploit them to control the kinetics, pathways and length of supramolecular polymers (SPs). New bisamide-containing monomers were designed to elucidate the role of competing intra- vs. intermolecular H-bonding interactions on the kinetics of supramolecular polymerization (SP). Remarkably, two polymerization-inactive metastable states were discovered. Contrary to previous examples, the commonly assumed intramolecularly H-bonded monomer does not evolve into intermolecularly H-bonded SPs via ring opening, but rather forms a metastable dimer. In this dimer, all H-bonding sites are saturated, either intra- or intermolecularly, hampering elongation. The dimers exhibit an advantageous preorganization, which upon opening of the intramolecular portion of the H-bonding motif facilitates SP in a consecutive process. The retardation of spontaneous self-assembly as a result of two metastable states enables length control in SP by seed-mediated growth.

Introduction

Hydrogen bonds (H-bonds) play a crucial role in a plethora of physico- and biochemical processes in nature, including the anomalous properties of water,[1] the stabilization of DNA double strands,[2] protein folding,[3] substrate-specific enzyme recognition[4] or ion transport through cell membranes,[5] among others.[6] The diversity of the processes in which H-bonds are involved can be correlated to their versatile nature, strength and directionality.[7] Inspired by their unique properties, researchers have investigated and exploited H-bonds in different fields, such as targeted drug delivery,[8] liquid crystals,[9] crystal engineering,[10] (asymmetric) catalysis[11] and others.[12] In the field of self-assembly, H-bonding motifs are commonly used supramolecular synthons that facilitate the formation of ordered and highly stable (co-)assemblies.[13] Furthermore, their combination with other secondary interactions in an orthogonal manner represents a powerful method to promote a cooperative growth.[14]

Even though H-bonds have been used for more than three decades in supramolecular polymerization (SP), it has not been until recently when their role on kinetically controlled self-assembly has been examined.[15,16–20] In his context, the development of monomer units that are able to engage in competing intra- and intermolecular H-bonding interactions has represented a key strategy for pathway and length control in SP.[20–22] In these systems, the formation of kinetically stable pseudo-cyclic conformations stabilized by intramolecular H-bonds (M*, Scheme 1a) hampers the establishment of an extended network of intermolecular H-bonds, which in turn retards polymer elongation. This initial

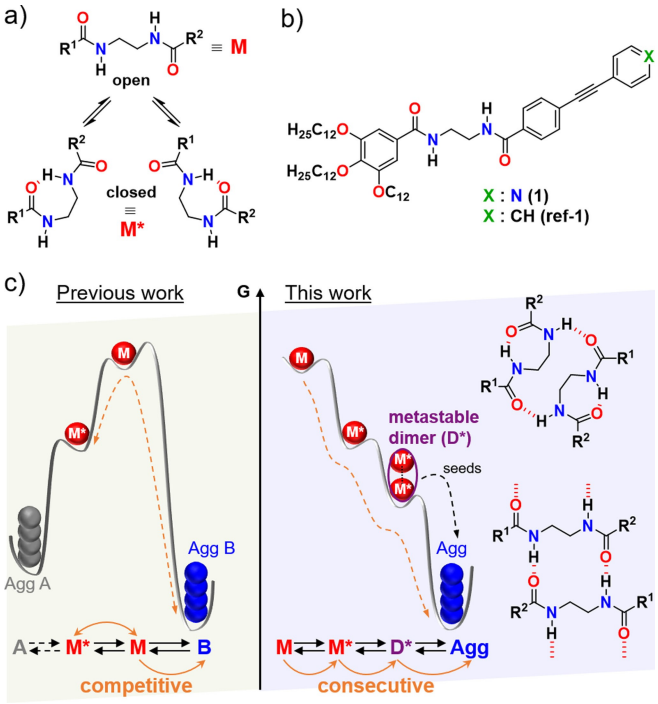

Scheme 1. a) Intramolecular H-bonding of bisamides yielding pseudo-cycles. b) Molecular structure of bisamides **1** and **ref-1**. c) Schematic energy landscapes illustrating the competitive aggregation pathways usually observed for intramolecularly H-bonded, metastable monomers (M*, and aggregates A) and the consecutive aggregation of an all-intermolecularly H-bonded SP from M* via the formation of a closed dimer (D*) with *intra-* and *inter*molecular H-bonds.

[*] J. Matern, Dr. Z. Fernández, N. Bäumer, Prof. Dr. G. Fernández
Organisch-Chemisches Institut,
Westfälische Wilhelms-Universität Münster
Corrensstraße 36, 48149 Münster (Germany)
E-mail: fernandg@uni-muenster.de

trapping affects various properties of the supramolecular system (e.g. chirality),[18,21,23] and can be exploited to spatiotemporally control the self-assembly, for example by seed-induced or living SP.[19,24] In recent years, the development of several molecular design strategies based on the formation of intramolecularly H-bonded pseudo-cycles has allowed to gain important insights into structure–property relationships, such as the length and nature of the linkers spacing the H-bonding sites.[16,25–27] In all of these studies, the competitive formation of a kinetically formed pseudo-cyclic monomer conformation via intramolecular H-bonds (M* in Scheme 1c, left) has been postulated as the main reason for the retardation of the SP. Apart from intramolecular H-bonds, other strategies for controlled SP based on the retardation of spontaneous self-assembly include the chemical (de-)activation[28] or light-induced conformational changes in the monomer state.[29] The vast majority of approaches where the kinetic species serving as SP feedstock is not a monomeric species rely on the formation of competitive/off-pathway aggregates. Strategies to spatiotemporally control SP through intermediates formed in a consecutive process are less explored[30] and especially small, discrete supramolecular intermediates,[31] which might be beneficial for size-limited systems, are underdeveloped in this context.

We herein examine the self-assembly of an unsymmetrical pyridine-based building block **1** bearing bisamide groups and solubilizing alkoxy chains (Scheme 1b). Additionally, to exclude a contribution of secondary interactions of the pyridyl moiety to the kinetics of the SP and thus be able to generalize our findings, control experiments with a new benzyl-substituted analogue (**ref-1**) were performed (see the Supporting Information). Interestingly, we discover an unprecedented sequence of self-assembly events leading to a complex energy landscape that contrasts with the current state of knowledge: we unravel a new metastable, H-bonded dimeric species (D*) incorporating both intra- and intermolecular H-bonds, which further extends the polymerization-inactive regime. The ideal preorganization of intra- and intermolecular H-bonds in D* enables the consecutive transformation of the initial intramolecularly H-bonded pseudo-cyclic monomers (M*) into intermolecularly H-bonded SPs without the need of significant molecular reorganizations. Ultimately, the seeded-growth approach was successfully applied to the metastable dimers, enabling precise control over the dimensions of the SPs. Our results introduce a new molecular design strategy for spatiotemporal control not only over the dimensions of SPs, but also over the size of the kinetic/metastable intermediates, thus broadening the scope of controlled SP.

Results and Discussion

Thermodynamic and Kinetic Self-Assembly Studies

In order to examine the experimental conditions under which **1** self-assembles, solvent-dependent UV/Visible (UV/Vis) studies were performed. At a concentration of 20 μM, characteristic absorption bands originating from π→π* transitions are observed between 250–325 nm in a variety of solvents that typically favor a molecularly dissolved state ($CHCl_3$, DCE, DCM, Figure 1a and Figure S2). Despite some minor changes in intensity, using methylcyclohexane (MCH, cyan spectrum) as typical aggregation-inducing solvent does not affect the position of the absorption maxima (292 nm and 310 nm) or the spectral pattern. Even if the concentration is raised by one order of magnitude (200 μM, dotted blue spectrum), still the spectral characteristics resemble those of monomeric **1** in good solvents. However, upon ageing (solid blue spectrum), H-type aggregation occurs in MCH, as suggested by the hypsochromic shift of the absorption maximum to 276 nm and the decrease in intensity of the maximum at 310 nm.[32] Such a retardation of the spontaneous SP in MCH points to the presence of a kinetically controlled species, presumably featuring intramolecular H-bonds.[16,20,25,33]

Atomic force microscopy (AFM) and scanning electron microscopy (SEM) revealed the formation of extended fibers exhibiting a strong tendency to bundle, both under dilute (Figure 1b and Figure S3) and concentrated conditions in MCH after equilibration (Figure 1c and Figure S4). These bundles can reach heights of several hundreds of nm and widths of several microns, while the smallest fibers were determined to have a height of approximately 5 nm and a width of ≈50 nm (for details see Figure S3). At millimolar concentrations, this bundling leads to the formation of an extended network of interconnected fibers, causing gelation (Figure 1c and Figure S3).

Temperature-dependent spectroscopy studies at different concentrations and cooling rates were carried out to elucidate the self-assembly mechanism. The variable temperature (VT)-UV/Vis spectra of **1**, registered between 368 K and 278 K at a rate of 1 $Kmin^{-1}$, show a two-stage transition upon cooling (Figure 2a and S1): during the initial temperature decrease to 288 K, the overall intensity slightly increases, accompanied by a small bathochromic shift of the absorption maxima by 2–3 nm (process A, Figure S1b). Apart from this, no changes in the spectral shape occur. Subsequently, the spectral features change drastically upon

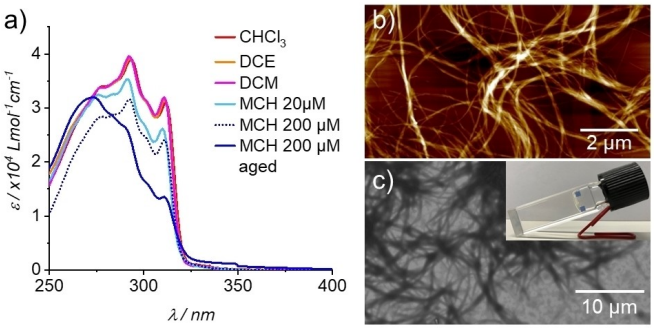

Figure 1. a) UV/Vis absorption spectra of **1** recorded in different solvents (if not stated otherwise: $c = 20$ μM, $T = 298$ K). b) AFM image of fibrous aggregates of **1** in MCH at $c = 40$ μM. c) SEM image of a xerogel of **1** in MCH ($c = 2$ mM) and photograph of the gel.

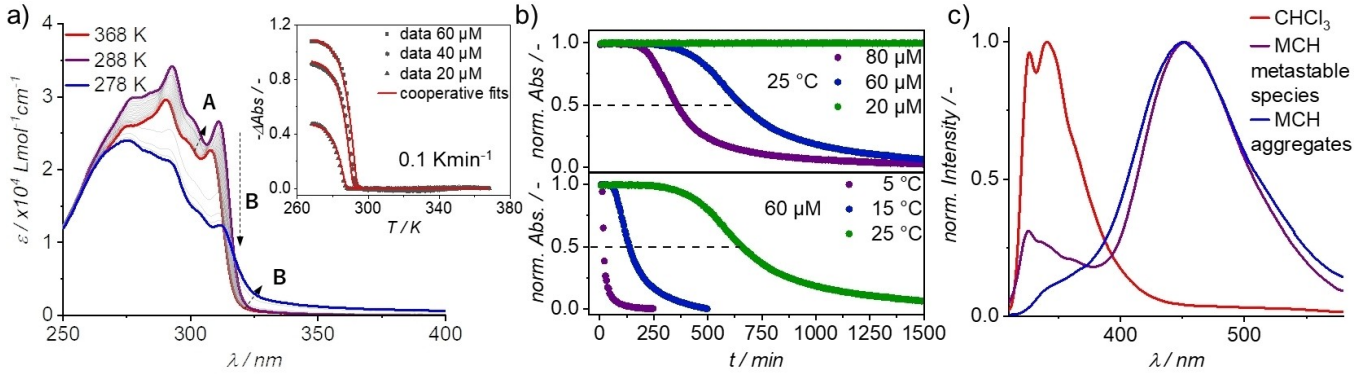

Figure 2. a) VT-UV/Vis absorption spectra upon cooling a solution of **1** in MCH ($c = 200\ \mu M$, $1\ K\,min^{-1}$). Inset: aggregation plots and cooperative fit curves at different concentrations at a cooling rate of $0.1\ K\,min^{-1}$ ($\lambda = 290$ nm). b) Kinetic profiles of aggregate formation over time ($\lambda = 292$ nm) after rapidly cooling a hot monomer solution at different concentrations (top) and different temperatures (bottom). c) Emission spectra ($\lambda_{exc.} = 292$ nm, $T = 298$ K) of **1** in the monomer state (red, $c = 20\ \mu M$), the metastable regime (purple, $c = 20\ \mu M$) and the aggregated state (blue, $c = 1$ mM), normalized to the highest intensity.

further cooling to 278 K, resulting in the spectra of the aggregated species (process B). Plotting the absorption at a given wavelength against the temperature yields non-sigmoidal curves, which could be fitted to the nucleation-elongation model (inset in Figure 2a, Figure S1),[34] revealing a cooperative polymerization mechanism. Successive cycles of cooling and heating of the same solution result in a large thermal hysteresis, which is strongly affected by the applied cooling rate (Figure S5). Remarkably, even at the slowest cooling rate ($0.1\ K\,min^{-1}$), which should favor a thermodynamically controlled self-assembly, a pronounced hysteresis is still observed. Altogether, this behavior is characteristic for the formation of metastable species, which retard spontaneous self-assembly. For this reason, the thermodynamic parameters derived from fitting the cooling curves, even at the slowest rate, possibly do not accurately describe the SP process (for details see the Supporting Information).

The kinetic evolution of the self-assembly after rapid cooling was monitored over time to gain insights into the effect of concentration and temperature on the metastable regime. This should allow a characterization of the metastable species as consecutive (on-pathway) or competitive (off-pathway) with respect to the thermodynamically stable SPs.[35] In the literature, two scenarios for the concentration-dependency are typically found: if the metastable species is a trapped monomer conformation (e.g. via intramolecular H-bonds, such as M*), the acceleration of the transformation upon increasing concentration is diagnostic of a competitive process.[20,25] In contrast, when the metastable species is a trapped aggregate instead of a monomer, an acceleration at higher concentrations is characteristic for a consecutive transformation.[25,26] Figure 2b shows the development of the absorption of **1** over time at different concentrations (top) and temperatures (bottom). Analogous experiments for **ref-1** are shown in Figure S6. An increase in concentration results in a faster formation of the supramolecular polymers, whereas the temperature has the inverse effect. Considering that our molecular design can satisfy both of the previously described scenarios (the metastable species can be either an aggregate or an intramolecularly H-bonded monomer M*), the observed temperature and concentration effects on the kinetic profiles could be explained in two different ways: i) The formation of a metastable monomer species in a competitive process; ii) the formation of a kinetically controlled aggregate that is a precursor of the thermodynamic polymer in a consecutive pathway. Dynamic light scattering (DLS), AFM and SEM studies showed that no defined nanostructures were formed in the initial lag phase, whereas networks of elongated fibers were detected after thermodynamic equilibration (Figure S7), which would suggest the competitive metastable monomer case.

Furthermore, emission studies were carried out (Figure 2c and Figure S8). The monomer species of **1** in $CHCl_3$ (red spectrum) is characterized by an emission band with vibronic features located between 340–350 nm, which is commonly observed for OPE-based compounds.[30,34] In stark contrast, solutions of the aggregated species show a broad emission at 450 nm (see royal blue spectrum in Figure 2c). Remarkably, the fluorescence spectrum of the metastable species recorded in the lag phase after initial cooling of a hot solution of **1** in MCH (step A in Figure 2a, purple spectrum) closely resembles that of the aggregated species, exhibiting a similar featureless emission around 450 nm. This observation is surprising, considering that in the lag phase no ordered, elongated structures are present (see previous UV/Vis, DLS and AFM experiments, Figure S7). To elucidate the origin of the emission band around 450 nm, we performed a filtration experiment: first, a solution in the lag phase (prepared by instant cooling from 368 K to 298 K) and in the aggregated state (prepared by slow cooling), were characterized by absorption and emission studies, respectively. Subsequently, the solutions were filtered through a syringe filter (0.2 µm) in order to exclusively remove the aggregate fibers (Figure S9). Despite some changes in the absorption spectra of the solution containing aggregates (→ removal of the aggregates), the emission spectra of both solutions were practically unaltered

after filtration. This indicates that the emission at 450 nm originates from a small-sized species which does not yet form elongated structures (for a detailed discussion, see the Supporting Information).

It has been widely established in the recent past that the formation of a pseudo-cycle by means of intramolecular H-bonding can trap monomers in a metastable, polymerization-inactive conformation. For both, **1** and **ref-1**, the equilibrium between open and closed conformations has been proposed based on VT- and concentration-dependent ^{1}H nuclear magnetic resonance (NMR) studies in $CDCl_3$ (Figures S10 and S11). However, corresponding VT-fluorescence studies only exhibit a change in the intensity of the previously observed monomer emission band (λ_{max} ≈340–350 nm) in the open-closed equilibrium, but no signs of the broad emission at ≈450 nm. Hence, the emission spectra of the metastable species recorded in the lag phase in time-dependent studies (λ_{max}≈450 nm) do not originate from a pseudo-cyclic monomer conformation, but rather from a different, discrete species. On this basis, the assumption of a competitive process between the closed monomer and the elongated polymer can be ruled out, thereby making a consecutive process the most plausible event.

Elucidation of the Supramolecular Species

To unravel the structures of the different species with respect to their molecular packing and the interactions dictating the respective arrangement, a combination of UV/Vis-absorption, emission, NMR and Fourier-transform infrared spectroscopy (FTIR) studies was carried out (Figures 3 and S12–S16). Starting at the open/pseudo-cyclic monomer equilibrium in $CDCl_3$ at RT, the amount of aggregation-inducing MCH-d_{14} in the solution was gradually increased. Up to an MCH fraction of approx. 40 %, a linear deshielding (absence of cooperative effects) of the amide resonances

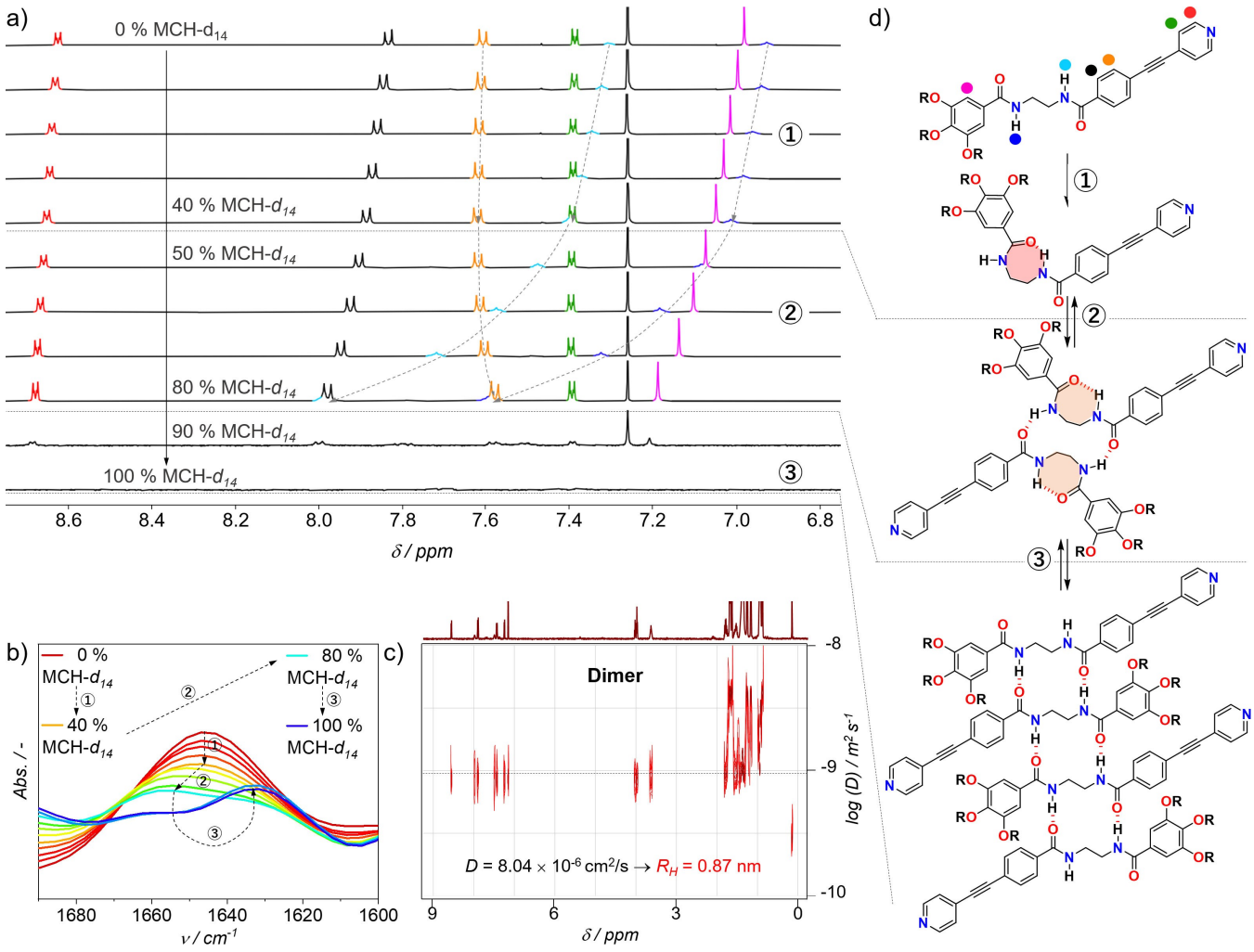

Figure 3. a) ^{1}H NMR studies of **1** upon stepwise increasing the volume fraction of MCH-d_{14} starting from 100% $CDCl_3$ (T=298 K, c=2 mM). b) Corresponding FTIR spectra in the carbonyl stretching region. c) DOSY ^{1}H NMR recorded in the metastable regime (MCH-d_{14}, T=353 K, c=2 mM). d) Schematic illustration of the multi-step polymerization mechanism. The dashed grey lines between (a) and (d) should guide the eye between the NMR spectra in (a) and the corresponding regime of the mechanism depicted in (d) that is probed in the experiment.

(blue + cyan), the protons of the trialkoxy-substituted phenyl ring (pink) and the protons in *ortho* position of the OPE phenyl ring with respect to the carbonyl (black) is observed (Figure 3a). On the other hand, the resonances of the pyridine protons (red and green) are negligibly affected. These changes are in line with a further shift of the open-closed equilibrium towards the intramolecularly H-bonded pseudo-cyclic monomer conformation (process ①). This is confirmed by the wavenumber of the carbonyl stretching observed in FTIR under equal conditions ($\nu_{C=O} = 1647\ cm^{-1}$, Figure 3b), diagnostic of the equilibrium between the open form and the intramolecularly H-bonded pseudo-cyclic form. Moreover, in the region of the N–H stretching vibration, two bands are registered: one characteristic for free N–H groups ($3453\ cm^{-1}$) and another one typical of intramolecularly H-bonded N–H groups ($3348\ cm^{-1}$) (Figure S12b).[36] On the other hand, in the regime between 50 % and 80 % MCH-d_{14}, the developments of the spectroscopic characteristics change (process ②). In NMR experiments, the resonance shifts are more pronounced and no longer linear (rise of cooperative effects), especially for the amide groups and the protons of the trialkoxy-substituted phenyl ring. Remarkably, the resonance of the OPE protons adjacent to the amide (orange) reverses its shift direction, starting to shield. Concomitantly, the amide I carbonyl band in the FTIR spectra splits into two bands: the band characteristic for intramolecular H-bonding is weakened (from $1647\ cm^{-1}$ to $1656\ cm^{-1}$) and a less intense shoulder band at $1635\ cm^{-1}$ evolves, which can be attributed to intermolecular H-bonding. At the same time, the intensity of the intramolecularly H-bonded N–H stretching band is significantly increased and a shoulder at lower wavenumbers develops in the region where typically intermolecular H-bonds are observed (Figure S12b). Interestingly, the NMR signals are not broadening and the absorption spectral features are almost unaltered (Figure S12a), indicating that these developments originate from interactions in a non-polymeric state, namely some kind of discrete preorganized species, i.e. dimer or small oligomer. Further decreasing the polarity of the solvent mixtures causes the sudden broadening and disappearance of all NMR resonances (process ③), accompanied by the merging of the amide I bands at $1656\ cm^{-1}$ and $1635\ cm^{-1}$ into a single, intense band at $1631\ cm^{-1}$ (Figure 3a,b). In the N–H stretching region, a single band at $3278\ cm^{-1}$ appears (Figure S12b). The existence of two different processes (regime ② and ③) occurring in pure MCH is also supported by combined VT NMR, absorption and emission experiments (Figures S14–S16).

The fact that the pyridine protons experience a slight downfield shift during the self-assembly processes suggests that the intermolecular association of the chromophores occurs in an antiparallel fashion, primarily driven by intermolecular H-bonding, as recently observed for a structurally similar unsymmetrical pyridine-based compound.[35] Another plausible packing mode would be a parallel arrangement of the monomers, wherein the pyridine units of adjacent monomers would be stacked on top of one another. However, this packing would induce a shielding of the pyridine protons, which disagrees with our experimental findings. Therefore, an antiparallel packing would be a reasonable explanation for the experimental findings, which is supported by theoretical calculations (see below).

Whereas processes ① and ③ are well explained by the known open/pseudo-cyclic monomer equilibrium via intramolecular H-bonds and the subsequent SP driven by extended intermolecular H-bonds, an intermediate process ② has not been described in the literature. We tentatively assign this process to the formation of a closed dimer involving simultaneous intra- and intermolecular H-bonds (Figure 3d), based on the following evidence: 1) Diffusion ordered NMR spectroscopy (DOSY) measurements revealed the presence of very small structures (Figures 3c and S17), even at millimolar concentrations. 2) The strong deshielding of the amide resonances in NMR and the appearance of stretching bands characteristic for both intra- and intermolecular H-bonds, both in the carbonyl and N–H region of the FTIR spectra, agrees with a closed, intermolecularly H-bonded dimer at the expense of the free N–H groups (process ② in Figure 3d). Concomitantly, the size of the seven-membered pseudo-cycle is expanded due to the constraints imposed by the stronger intermolecular H-bonds ($\rightarrow \nu_{C=O}$ shifts from $1648\ cm^{-1}$ to $1656\ cm^{-1}$). 3) In the proposed dimer, the individual molecules are well preorganized to elongate into extended SPs without dissociation into the open monomer: only the intramolecular H-bond needs to be dissociated in favor of new intermolecular H-bonds (process ③), which is in line with a consecutive polymerization pathway, despite initial formation of the pseudo-cyclic monomer. 4) The energy barrier for the nucleation of all-intermolecularly H-bonded SPs is usually increased when another metastable intermediate exists in addition to the monomer.[25] Thus, the transformation to the intermolecularly H-bonded SPs should be accelerated at higher temperatures in the kinetic experiments (→ enabling opening of the closed conformation).[17] In contrast, in our case, a lower temperature is beneficial to surpass the metastable regime. This can be explained by the weakening of the intramolecular H-bonds as a result of the intermolecular H-bonds developed in the dimer, whose formation is favored at lower temperatures.

Computational Studies

DFT calculations (B3LYP/6-31(+)G(d,p)) of the different (supramolecular) species of **1** in MCH as solvent were carried out in order to further understand the intricate sequence of assembly events (Figures 4 and S21–S23). To reduce computational costs, the dodecyloxy side chains were shortened to methoxy groups. As the experimental data suggests that the SP is primarily conditioned by the different H-bonding patterns, the removal of the long alkyl chains for the calculations is anticipated to have a negligible impact on the simulated SP properties.

Initially, different monomer conformations of **1** were geometry-optimized in order to compare their relative stabilities. The DFT calculations revealed a stabilization of

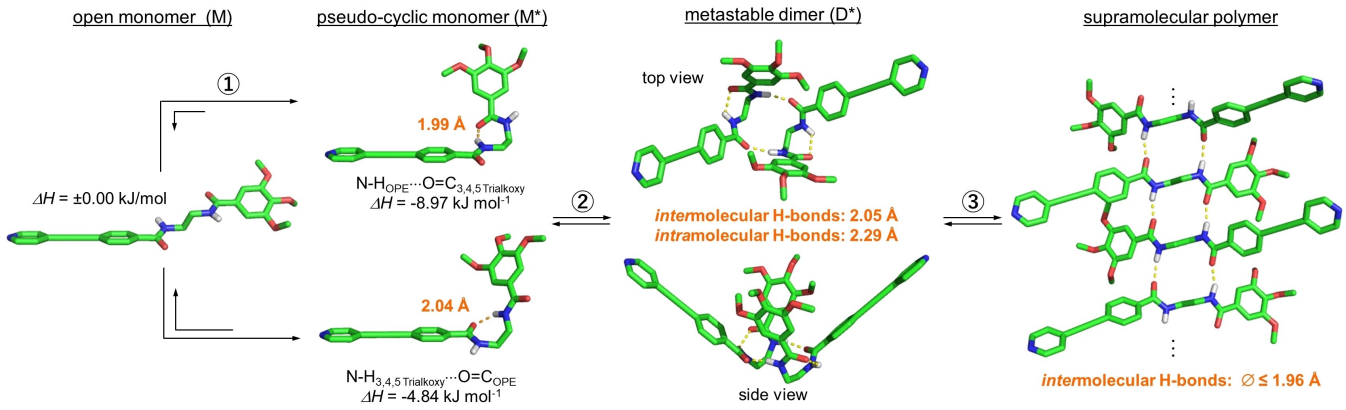

Figure 4. Sequence of self-assembly events of **1**, illustrated by the geometry-optimized structures of different (supra)molecular species obtained by DFT calculations (B3LYP/6-31(+)G(d,p)).

$-8.97\ kJ\,mol^{-1}$ through intramolecular H-bonding in a pseudo-cyclic conformation when compared to the open form (Figures 4 and S21). Given the two possible intramolecular H-bonding connectivities in a pseudo-cyclic form (both amides can either act as H-bond donor or acceptor giving rise to two conformers), the two possible conformations were optimized. The calculations predict that the more stable pseudo-cyclic conformation is established between the carbonyl of the 3,4,5-trialkoxybenzamide and the OPE-bound amide proton, as depicted in Figures 3 and 4. This conformer was subsequently used as a starting point for the optimization of the metastable cyclic dimer species (D*), which was proposed based on the experimental results. Notably, DFT optimizations of a dimer species D* bearing both intra- and intermolecular H-bonding interactions corroborated that this interaction pattern is feasible (Figures 4 and S22c–e). To computationally quantify the relative stability of this closed dimer conformation, we also optimized the geometries of other plausible dimer structures with either parallel or antiparallel molecular arrangements in which only intermolecular H-bonds are possible (Figure S22a,b). Interestingly, the proposed closed dimer D* is superiorly stabilized in comparison to both the antiparallel and parallel dimers by $\Delta H = -6.19\ kJ\,mol^{-1}$ and $\Delta H = -11.95\ kJ\,mol^{-1}$, respectively. Moreover, the expansion of the pseudo-cycle in the metastable dimer was confirmed, as proposed based on the wavenumbers of the amide I C=O stretching band in FTIR: the intramolecular N–H···O=C distance increases from 1.99 Å in the metastable monomer (M*) to 2.29 Å in D*.

Additionally, we also examined the most plausible molecular packing in the all- intermolecularly H-bonded SPs by DFT calculations. To this end, the previously described parallel and antiparallel dimers were used to grow trimers and tetramers with the respective arrangement (Figure S23). In line with previous results, the calculations rendered a lower energy for the antiparallel orientation when compared to the parallel alignment (Table S2). In good accordance with the conclusions drawn from the NMR studies and the literature,[37] the calculations provide a reasonable explanation for the preferred formation of the antiparallel over the parallel arrangements: as a consequence of the unsymmetrical molecular design, an unfavorable macroscopic dipole moment would build up upon elongation in a hypothetical parallel arrangement, whereas in the antiparallel stacking mode, the dipole moment is much lower (see Figure S23e,f and μ Table S2).

As expected, the intermolecular H-bonds in the antiparallel packing mode become stronger upon elongating the stack, which is reflected in the decreasing average intermolecular N–H···O=C distance: 2.05 Å (D*)→1.97 Å (antiparallel trimer)→1.96 Å (antiparallel tetramer). Furthermore, the cooperative character of the SP is supported by the increasing absolute values of the stabilization energy per monomer addition step (ΔE_{avg} in Table S2).[17,38]

Seed-Induced Supramolecular Polymerization

Having clarified the steps involved in the self-assembly of **1**, we explored the possibility of a seed-induced SP (SSP) using the metastable dimer as monomer reservoir/polymerization feedstock. Polymer seeds with lengths between 50–200 nm were fabricated via sonication of the supramolecular polymers obtained in stage ③ (Figure S18a,b). Subsequently, these seeds were added to solutions that were thermally quenched by instant cooling from 368 K to 298 K (→ metastable dimers are formed) and the seeded growth was monitored by atomic force microscopy (AFM). Pleasingly, SP is instantly initiated and a rapid transformation to large, elongated fibers within one hour takes place (Figure S18c,d). The seed-mediated growth allowed us to control the length of the SP fibers in a living manner through adjusting the [seed]/[metastable] ratio (see AFM images in Figure 5 and S19): upon increasing the amount of metastable feedstock solution leading to ratios of 1:1 to 1:2, 1:5 and 1:10, the length of the polymer strands grew linearly from an average of 392 nm to 6381 nm (for details see also Figure S19). Note that the small, bright artifacts in images (a)–(c) and (e)–(g) are nanoscopic glass particles released from the cuvettes, which do not affect the SSP (for details see the Supporting Information). Furthermore, repeated cycles of adding **1** in

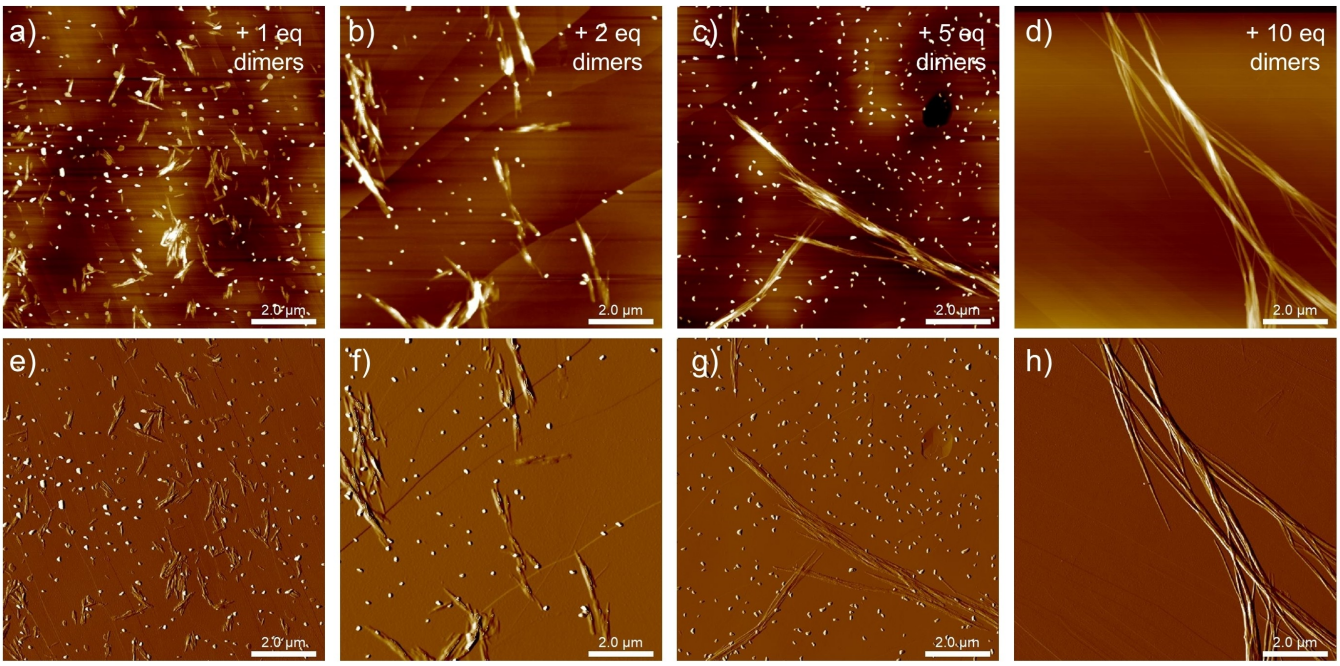

Figure 5. AFM images of seed-induced supramolecular polymerization (SSP) of **1** through controlling the [seed]:[metastable feedstock] ratio. a)–d) Height images. e)–h) Corresponding phase images. Solution condition prior to drop-casting the samples onto HOPG: $c = 20\ \mu M$, $T = 298\ K$; ratios [seed]:[metastable]: a), e) 1:1, b), f) 1:2, c), g) 1:5, d), h) 1:10.

the metastable state to an invariant amount of polymer seeds also allowed to gradually increase the size of the nanostructures in a stepwise manner (Figure S20). Consequently, the D* dimers represent an ideal intermediate for size control in SP, as they extend the time window of the metastable regime while simultaneously responding instantly to the addition of seeds.

Conclusion

In conclusion, our detailed investigations on the self-assembly of the compounds **1** and **ref-1** have brought to light the existence of a previously unknown metastable species in the supramolecular self-assembly of hydrogen bonding synthons. Initially, bisamide-containing building blocks **1** and **ref-1** equilibrate between an open, linear form and pseudo-cyclic monomer conformations stabilized by intramolecular H-bonds. Interestingly, in sharp contrast to the current state-of-the-art in the literature, the pseudo-cyclic conformation does not dissociate into the open monomer to initiate extended SP. Instead, it undergoes a subsequent dimerization to form an unprecedented metastable dimer species (D*) that incorporates both intra- as well as intermolecular H-bonds between the amide units. Interestingly, D* serves as a precursor for the formation of the all-intermolecularly H-bonded, thermodynamic supramolecular polymer. For this reason, the usual observation of a competitive formation of intermolecularly H-bonded SPs with respect to the pseudo-cycle monomer (→ closed monomers have to be converted into open monomers first), is turned into a consecutive process. Nevertheless, the intermediate formation of the dimer retards the evolution of elongated SPs, resulting in a polymerization-inactive, metastable regime, which can be exploited to perform seed-mediated living polymer growth.

Our work not only broadens the scope of kinetically controlled SP, but also highlights the relevance of complex hydrogen bonding patterns in controlling the kinetic outcome of self-assembly processes. In our view, close research scrutiny of H-bonded assemblies is required to tackle this challenge.

Acknowledgements

J.M. thanks the "Verband der Chemischen Industrie" for a Kekulé PhD fellowship and the Deutsche Forschungsgemeinschaft (DFG, CRC 1450 inSight-431460824) for further funding. Z.F. thanks Xunta de Galicia for a Postdoctoral fellowship. G.F. and N.B. gratefully acknowledge the European Research Council (ERC-StG-2016 SUPRACOP-715923) and the DFG (IRTG 2678) for funding. We acknowledge Cesga for computational time. Open Access funding enabled and organized by Projekt DEAL.

Conflict of Interest

The authors declare no conflict of interest.

Data Availability Statement

The data that support the findings of this study are available in the Supporting Information of this article.

Keywords: Hydrogen Bonding · Kinetic Effects · π-Conjugated Systems · Self-Assembly · Supramolecular Polymerization

[1] A. Nilsson, L. G. M. Pettersson, *Nat. Commun.* **2015**, *6*, 8998.
[2] J. D. Watson, F. H. C. Crick, *Nature* **1953**, *171*, 737–738.
[3] a) P. W. Hildebrand, S. Günther, A. Goede, L. Forrest, C. Frömmel, R. Preissner, *Biophys. J.* **2008**, *94*, 1945–1953; b) A.-N. Bondar, S. H. White, *Biochim. Biophys. Acta Biomembr.* **2012**, *1818*, 942–950; c) J. U. Bowie, *Curr. Opin. Struct. Biol.* **2011**, *21*, 42–49; d) S. H. White, *Advances in Protein Chemistry: Peptide Solvation and H-Bonds*, Academic Press, New York, **2005**, pp. 157–172.
[4] a) V. S. Bhatt, W. Guan, M. Xue, H. Yuan, P. G. Wang, *Biochem. Biophys. Res. Commun.* **2011**, *412*, 232–237; b) F. Forouhar, J. L. R. Anderson, C. G. Mowat, S. M. Vorobiev, A. Hussain, M. Abashidze, C. Bruckmann, S. J. Thackray, J. Seetharaman, T. Tucker, R. Xiao, L.-C. Ma, L. Zhao, T. B. Acton, G. T. Montelione, S. K. Chapman, L. Tong, *Proc. Natl. Acad. Sci. USA* **2007**, *104*, 473–478.
[5] a) R. Dutzler, E. B. Campbell, R. MacKinnon, *Science* **2003**, *300*, 108–112; b) L. E. Bickerton, A. J. Sterling, P. D. Beer, F. Duarte, M. J. Langton, *Chem. Sci.* **2020**, *11*, 4722–4729.
[6] G. Gilli, P. Gilli, *The Nature of the Hydrogen Bond*, Oxford University Press, New York, **2009**.
[7] a) P. Gilli, L. Pretto, V. Bertolasi, G. Gilli, *Acc. Chem. Res.* **2009**, *42*, 33–44; b) E. Arunan, G. R. Desiraju, R. A. Klein, J. Sadlej, S. Scheiner, I. Alkorta, D. C. Clary, R. H. Crabtree, J. J. Dannenberg, P. Hobza, H. G. Kjaergaard, A. C. Legon, B. Mennucci, D. J. Nesbitt, *Pure Appl. Chem.* **2011**, *83*, 1637–1641.
[8] a) Y. Shi, T. Lammers, G. Storm, W. E. Hennink, *Macromol. Biosci.* **2017**, *17*, 1600160; b) J. Boucard, C. Linot, T. Blondy, S. Nedellec, P. Hulin, C. Blanquart, L. Lartigue, E. Ishow, *Small* **2018**, *14*, 1802307.
[9] a) C. M. Paleos, D. Tsiourvas, *Angew. Chem. Int. Ed. Engl.* **1995**, *34*, 1696–1711; *Angew. Chem.* **1995**, *107*, 1839–1855; b) C. M. Paleos, D. Tsiourvas, *Liq. Cryst.* **2001**, *28*, 1127–1161.
[10] a) A. D. Burrows, C.-W. Chan, M. M. Chowdhry, J. E. McGrady, D. M. P. Mingos, *Chem. Soc. Rev.* **1995**, *24*, 329; b) C. B. Aakeröy, K. R. Seddon, *Chem. Soc. Rev.* **1993**, *22*, 397–407; c) S. Subramanian, M. J. Zaworotko, *Coord. Chem. Rev.* **1994**, *137*, 357–401.
[11] a) P. R. Schreiner, *Chem. Soc. Rev.* **2003**, *32*, 289–296; b) L. Zu, J. Wang, H. Li, H. Xie, W. Jiang, W. Wang, *J. Am. Chem. Soc.* **2007**, *129*, 1036–1037; c) P. M. Pihko, *Angew. Chem. Int. Ed.* **2004**, *43*, 2062–2064; *Angew. Chem.* **2004**, *116*, 2110–2113; d) L. Bouteiller, M. Raynal in *Supramolecular Catalysis* (Eds.: P. W. van Leeuwen, M. Raynal), Wiley, Hoboken, **2022**.
[12] a) L. J. Prins, D. N. Reinhoudt, P. Timmerman, *Angew. Chem. Int. Ed.* **2001**, *40*, 2382–2426; *Angew. Chem.* **2001**, *113*, 2446–2492; b) Z. Fernández, B. Fernández, E. Quiñoá, F. Freire, *J. Am. Chem. Soc.* **2021**, *143*, 20962–20969.
[13] a) L. Brunsveld, B. J. B. Folmer, E. W. Meijer, R. P. Sijbesma, *Chem. Rev.* **2001**, *101*, 4071–4098; b) Y. Li, A. Hammoud, L. Bouteiller, M. Raynal, *J. Am. Chem. Soc.* **2020**, *142*, 5676–5688; c) S. Han, S. Pensec, D. Yilmaz, C. Lorthioir, J. Jestin, J.-M. Guigner, F. Niepceron, J. Rieger, F. Stoffelbach, E. Nicol, O. Colombani, L. Bouteiller, *Nat. Commun.* **2020**, *11*, 4760; d) G. Basuyaux, A. Desmarchelier, G. Gontard, N. Vanthuyne, J. Moussa, H. Amouri, M. Raynal, L. Bouteiller, *Chem. Commun.* **2019**, *55*, 8548–8551; e) A. Jamadar, A. Das, *Polym. Chem.* **2020**, *11*, 385–392; f) S. Cantekin, T. F. A. de Greef, A. R. A. Palmans, *Chem. Soc. Rev.* **2012**, *41*, 6125–6137; g) A. Das, S. Ghosh, *Chem. Commun.* **2016**, *52*, 6860–6872; h) A. Das, G. Vantomme, A. J. Markvoort, H. M. M. ten Eikelder, M. Garcia-Iglesias, A. R. A. Palmans, E. W. Meijer, *J. Am. Chem. Soc.* **2017**, *139*, 7036–7044; i) C. M. A. Leenders, M. B. Baker, I. A. B. Pijpers, R. P. M. Lafleur, L. Albertazzi, A. R. A. Palmans, E. W. Meijer, *Soft Matter* **2016**, *12*, 2887–2893; j) Z. Fernández, B. Fernández, E. Quiñoá, F. Freire, *Angew. Chem. Int. Ed.* **2021**, *60*, 9919–9924; *Angew. Chem.* **2021**, *133*, 10007–10012.
[14] a) C. Rest, R. Kandanelli, G. Fernández, *Chem. Soc. Rev.* **2015**, *44*, 2543–2572; b) C. A. Hunter, H. L. Anderson, *Angew. Chem. Int. Ed.* **2009**, *48*, 7488–7499; *Angew. Chem.* **2009**, *121*, 7624–7636.
[15] a) M. Wehner, M. I. S. Röhr, M. Bühler, V. Stepanenko, W. Wagner, F. Würthner, *J. Am. Chem. Soc.* **2019**, *141*, 6092–6107; b) A. Sarkar, R. Sasmal, A. Das, S. S. Agasti, S. J. George, *Chem. Commun.* **2021**, *57*, 3937–3940; c) A. Mishra, S. Dhiman, S. J. George, *Angew. Chem. Int. Ed.* **2021**, *60*, 2740–2756; *Angew. Chem.* **2021**, *133*, 2772–2788; d) A. Mishra, D. B. Korlepara, M. Kumar, A. Jain, N. Jonnalagadda, K. K. Bejagam, S. Balasubramanian, S. J. George, *Nat. Commun.* **2018**, *9*, 1295; e) G. Ghosh, R. Barman, A. Mukherjee, U. Ghosh, S. Ghosh, G. Fernández, *Angew. Chem. Int. Ed.* **2022**, *61*, e202113403; *Angew. Chem.* **2022**, *134*, e202113403; f) A. Sikder, S. Ghosh, *Mater. Chem. Front.* **2019**, *3*, 2602–2616; g) A. Chakraborty, R. N. Manna, A. Paul, S. Ghosh, *Chem. Eur. J.* **2021**, *27*, 11458–11467; h) K. Venkata Rao, D. Miyajima, A. Nihonyanagi, T. Aida, *Nat. Chem.* **2017**, *9*, 1133–1139; i) B. Adelizzi, I. A. W. Filot, A. R. A. Palmans, E. W. Meijer, *Chem. Eur. J.* **2017**, *23*, 6103–6110; j) A. Isobe, D. D. Prabhu, S. Datta, T. Aizawa, S. Yagai, *Chem. Eur. J.* **2020**, *26*, 8997–9004; k) A. Suzuki, K. Aratsu, S. Datta, N. Shimizu, H. Takagi, R. Haruki, S. Adachi, M. Hollamby, F. Silly, S. Yagai, *J. Am. Chem. Soc.* **2019**, *141*, 13196–13202; l) T. Aizawa, S. Takahashi, A. Isobe, S. Datta, H. Sotome, H. Miyasaka, T. Kajitani, S. Yagai, *Chem. Lett.* **2020**, *49*, 1009–1012; m) K. Tamaki, S. Datta, K. Tashiro, A. Isobe, F. Silly, S. Yagai, *Asian J. Org. Chem.* **2021**, *10*, 257–261; n) V. Ayzac, Q. Sallembien, M. Raynal, B. Isare, J. Jestin, L. Bouteiller, *Angew. Chem. Int. Ed.* **2019**, *58*, 13849–13853; *Angew. Chem.* **2019**, *131*, 13987–13991; o) L. N. J. de Windt, Z. Fernández, M. Fernández-Míguez, F. Freire, A. R. A. Palmans, *Chem. Eur. J.* **2022**, *28*, e202103691.
[16] E. E. Greciano, S. Alsina, G. Ghosh, G. Fernández, L. Sánchez, *Small Methods* **2020**, *4*, 1900715.
[17] E. E. Greciano, J. Calbo, E. Ortí, L. Sánchez, *Angew. Chem. Int. Ed.* **2020**, *59*, 17517–17524; *Angew. Chem.* **2020**, *132*, 17670–17677.
[18] J. S. Valera, R. Gómez, L. Sánchez, *Angew. Chem. Int. Ed.* **2019**, *58*, 510–514; *Angew. Chem.* **2019**, *131*, 520–524.
[19] J. Kang, D. Miyajima, T. Mori, Y. Inoue, Y. Itoh, T. Aida, *Science* **2015**, *347*, 646–651.
[20] S. Ogi, V. Stepanenko, K. Sugiyasu, M. Takeuchi, F. Würthner, *J. Am. Chem. Soc.* **2015**, *137*, 3300–3307.
[21] M. Wehner, M. I. S. Röhr, V. Stepanenko, F. Würthner, *Nat. Commun.* **2020**, *11*, 5460.
[22] a) E. E. Greciano, L. Sánchez, *Chem. Eur. J.* **2016**, *22*, 13724–13730; b) S. Ogi, N. Fukaya, Arifin, B. B. Skjelstad, Y. Hijikata, S. Yamaguchi, *Chem. Eur. J.* **2019**, *25*, 7303–7307; c) A. Chakraborty, G. Ghosh, D. S. Pal, S. Varghese, S. Ghosh, *Chem. Sci.* **2019**, *10*, 7345–7351.
[23] C. Naranjo, Y. Dorca, G. Ghosh, R. Gómez, G. Fernández, L. Sánchez, *Chem. Commun.* **2021**, *57*, 4500–4503.
[24] a) M. Wehner, F. Würthner, *Nat. Chem. Rev.* **2020**, *4*, 38–53; b) S. Ogi, K. Sugiyasu, S. Manna, S. Samitsu, M. Takeuchi, *Nat.*

Chem. **2014**, *6*, 188–195; c) R. D. Mukhopadhyay, A. Ajayaghosh, *Science* **2015**, *349*, 241–242.
[25] S. Ogi, V. Stepanenko, J. Thein, F. Würthner, *J. Am. Chem. Soc.* **2016**, *138*, 670–678.
[26] E. E. Greciano, B. Matarranz, L. Sánchez, *Angew. Chem. Int. Ed.* **2018**, *57*, 4697–4701; *Angew. Chem.* **2018**, *130*, 4787–4791.
[27] E. E. Greciano, M. A. Martínez, S. Alsina, A. Laguna, L. Sánchez, *Org. Chem. Front.* **2021**, *8*, 5328–5335.
[28] a) S. Dhiman, R. Ghosh, S. Sarkar, S. J. George, *Chem. Sci.* **2020**, *11*, 12701–12709; b) K. Jalani, A. D. Das, R. Sasmal, S. S. Agasti, S. J. George, *Nat. Commun.* **2020**, *11*, 3967; c) A. Jain, S. Dhiman, A. Dhayani, P. K. Vemula, S. J. George, *Nat. Commun.* **2019**, *10*, 450.
[29] a) M. Endo, T. Fukui, S. H. Jung, S. Yagai, M. Takeuchi, K. Sugiyasu, *J. Am. Chem. Soc.* **2016**, *138*, 14347–14353; b) B. Adhikari, K. Aratsu, J. Davis, S. Yagai, *Angew. Chem. Int. Ed.* **2019**, *58*, 3764–3768; *Angew. Chem.* **2019**, *131*, 3804–3808.
[30] a) T. Fukui, S. Kawai, S. Fujinuma, Y. Matsushita, T. Yasuda, T. Sakurai, S. Seki, M. Takeuchi, K. Sugiyasu, *Nat. Chem.* **2017**, *9*, 493–499; b) A. Sarkar, R. Sasmal, A. Das, A. Venugopal, S. S. Agasti, S. J. George, *Angew. Chem. Int. Ed.* **2021**, *60*, 18209–18216; *Angew. Chem.* **2021**, *133*, 18357–18364; c) S. Sarkar, A. Sarkar, A. Som, S. S. Agasti, S. J. George, *J. Am. Chem. Soc.* **2021**, *143*, 11777–11787; d) S. Sarkar, A. Sarkar, S. J. George, *Angew. Chem. Int. Ed.* **2020**, *59*, 19841–19845; *Angew. Chem.* **2020**, *132*, 20013–20017.
[31] A. Sarkar, R. Sasmal, C. Empereur-Mot, D. Bochicchio, S. V. K. Kompella, K. Sharma, S. Dhiman, B. Sundaram, S. S. Agasti, G. M. Pavan, S. J. George, *J. Am. Chem. Soc.* **2020**, *142*, 7606–7617.
[32] a) N. J. Hestand, F. C. Spano, *Chem. Rev.* **2018**, *118*, 7069–7163; b) T. Rudolph, N. Kumar Allampally, G. Fernández, F. H. Schacher, *Chem. Eur. J.* **2014**, *20*, 13871–13875.
[33] H. Choi, S. Ogi, N. Ando, S. Yamaguchi, *J. Am. Chem. Soc.* **2021**, *143*, 2953–2961.
[34] a) H. M. M. ten Eikelder, A. J. Markvoort, T. F. A. de Greef, P. A. J. Hilbers, *J. Phys. Chem. B* **2012**, *116*, 5291–5301; b) A. J. Markvoort, H. M. M. ten Eikelder, P. A. J. Hilbers, T. F. A. de Greef, E. W. Meijer, *Nat. Commun.* **2011**, *2*, 509.
[35] J. Matern, Y. Dorca, L. Sánchez, G. Fernández, *Angew. Chem. Int. Ed.* **2019**, *58*, 16730–16740; *Angew. Chem.* **2019**, *131*, 16884–16895.
[36] a) S. H. Gellman, G. P. Dado, G. B. Liang, B. R. Adams, *J. Am. Chem. Soc.* **1991**, *113*, 1164–1173; b) J. S. Nowick, M. Abdi, K. A. Bellamo, J. A. Love, E. J. Martinez, G. Noronha, E. M. Smith, J. W. Ziller, *J. Am. Chem. Soc.* **1995**, *117*, 89–99.
[37] A. Jamadar, A. K. Singh, L. Roy, A. Das, *J. Mater. Chem. C* **2021**, *9*, 11893–11904.
[38] a) J. Buendía, J. Calbo, F. García, J. Aragó, P. M. Viruela, E. Ortí, L. Sánchez, *Chem. Commun.* **2016**, *52*, 6907–6910; b) M. A. Martínez, A. Doncel-Giménez, J. Cerdá, J. Calbo, R. Rodríguez, J. Aragó, J. Crassous, E. Ortí, L. Sánchez, *J. Am. Chem. Soc.* **2021**, *143*, 13281–13291; c) F. García, P. M. Viruela, E. Matesanz, E. Ortí, L. Sánchez, *Chem. Eur. J.* **2011**, *17*, 7755–7759.

Manuscript received: March 13, 2022
Accepted manuscript online: March 31, 2022
Version of record online: May 5, 2022